LEGENDA:

Corrosion-fatigue tests using strain gauges on the specimen to monitoring the load applied under specimen subject to high pressure.

Rodrigo R. A. Garcia[a], Alessandro S. de Lima[a], Yuri Laet Ramalho[b] , Felipe Cristaldi[b], Emannuel P. Q. Pereira[c], Sergio G. Tavares[d] , Oscar Rosa Mattos[e]

Abstract

This paper is using numeric analysis and experimental data to validate the use of strain gauges for load and crack propagation measurements in corrosion-fatigue. It was shown that the measurement of crack length and load by strain gauges can be done following the requirements of ASTM E647-15. The results open the possibility for using strain gauges directly positioned on the samples, replacing both: the classical load cells to measure load and direct current potential drop to determine fatigue crack growth rate, since neither are easily usable for high-pressure corrosion-fatigue tests.

Keywords: corrosion fatigue, fatigue crack growth rate, high pressure test, Back Face Strain – BFS, load cell, load measurement.

Introduction

Fatigue of metallic structures is a complex problem involving particularities of mechanic properties and microstructures of the material. In presence of a corrosive medium, the complexity of fatigue failure increases significantly, involving the particularities of the corrosion process. It is common to study this problem by using the da/dN versus ΔK curves, where da/dN is the fatigue crack growth rate (FCGR) and ΔK is the range of stress intensity factor. The correct methodology to obtain this curve imposes an accurate monitoring of the load and the crack length, as it is described in the standards (1, 2). The so-called direct current potential drop (DCPD) is commonly used to measure the crack length, and for tests in air condition, this technique is satisfactory. However, in presence of corrosive environment the imposed current for using DCPD can polarize the sample and increase or decrease FCGR (1,

[a] M. Sc., Researcher engineer - LNDC/UFRJ
[b] Graduate student of Engineering - UFRJ
[c] Research technician - LNDC/UFRJ
[d] Researcher engineer - LNDC/UFRJ
[e] D.Sc, Professor - UFRJ

3, 4). Another aspect regarding this technique in corrosion-fatigue tests is that it is more recommended to use two samples, one as work and other as reference and consequently, it will require connecting simultaneously eight wires for the passage of electrical current and the potential drop measurements (1). Therefore, it becomes difficult to adapt the setup of this technique for pressured tests in autoclave.
An alternative technique proposed at least 35 years ago is called back face strain gauge (BFS) (4-12). Despite the advantages of this technique, only recently, a mathematical equation was developed, allowing the use of BFS in a large crack length range and with a very satisfactory accuracy (5). Other point to be outlined is the quality of the adhesive to fix the BFS on the sample that has been improved lately. Concerning the measurement of applied load on the sample, load cells are currently used. However, for high-pressure fatigue test using autoclave setup, the external load cell normally does not measure the load correctly (4). In this case, the load cell must be located inside the autoclave, but it is not an easy setup. The standard ASTM E-1820 (13) proposes the use of strain gauges directly positioned in the sample to measure the applied load, but the details for doing it is not described in the standard.
In the present paper, a methodology of using strain gauges to monitor the crack propagation as well as the applied load in a compact tension specimen, C(T), in a corrosion-fatigue test is presented. The crack length measured by BFS was compared with the value measured by optical microscopy, as well as, the load obtained by the procedure used in this paper was compared with the values obtained by a calibrated load cell.

Method

C(T) specimens were machined from API X65 steel (table 1) and the dimensions are presented in figure 1, where B and W are respectively the thickness and width of the sample, a is the crack length measured from the reference plane to the crack tip and a_n is the machined notch length.

INSERT TABLE 1

INSERT FIGURE 1

Three different strain gauges were used; one uniaxial type, as traditionally used for crack length measurement by BFS, and the two others were biaxial type XY. The first was positioned on the upper face and the last one under the lower face forming a bridge, suitable to eliminate discrepancies in load measurement, such as those caused by a slight misalignment, see figure 2. Therefore, this pair of biaxial strain gauges will be called in this work as extreme face strain gauges (EFS). The features of the strain gauges are 3 mm length and resistance equals to 350 Ω.

INSERT FIGURE 2

The strain gauges on the samples were protected from corrosive environmental (figure 3) using two kinds of coatings: one elastomer and other ceramic coating, table 2 shows the characteristics of them. Both coatings are chemically inert in NaCl solutions and figure 3 presents the coated samples.

INSERT TABLE 2

INSERT FIGURE 3

A servo mechanic Instron 8801 was used to impose the fatigue load, obtaining the da/dN curves, a homemade software written in Labview ® embedded with a real-time industrial controller, Compact-Rio ®, made by National Instruments © recorded the data acquisition of load, crack length, stress intensity factor, strain gauge measurements and number of cycles.

Finite element analysis (FEA) procedure used for BFS calibration curve
Commercial software was used for finite element analysis, ANSYS 15.0. The element type used for structural analysis was a 20 node, 186 model. It is a higher order 3-D element that exhibits quadratic displacement behaviour. The element is defined by 20 nodes having three degree of freedom per node: translation in the nodal X, Y, and Z directions (14 – 16). The geometry of the element was tetrahedral (4 vertices), as it is shown in figure 4.

INSERT FIGURE 4

This setup is adequate to obtain the well-established singular stress field by shifting the mid-side nodes one-quarter away from the crack tip. Then, it is recommended to the problem of this work, since its scope applies to materials on linear elastic regime with irregular meshes for either isotropic, orthotropic or even anisotropic materials. The refining type containing 80471 nodes and 51249 elements was used, since the results are practically the same that it is achieved when a 3 times more refined mesh is used. Thus, the initial refining was validated to converge the results of FEA with the boundary conditions suggested, where the load applied has always respected the linear elastic regime (1, 2), see figure 5.

INSERT FIGURE 5

The geometric dimensions of the C(T) specimens were $W = 60\ mm\ ;\ B = 10\ mm$; for sixteen different crack lengths, $a/W = [0.20\ ;\ 0.95]$ *with* $0.05\ a/W$ ranges and the strain gauge dimension was 3 mm x 1.5 mm. Similar parameters to those detailed for BFS curves were used for EFS curves calibration, however, twelve strain gauges were placed simultaneously on the upper face, analysing the behaviour of compressive deformations undergone by them, as a function of applied load and of a predetermined crack length. Table 3 and figure 6 show further details of the strain gauge candidates.

INSERT TABLE 3

INSERT FIGURE 6

Results and discussion

Validation of BFS as method to measure the crack length.
Newman recently proposed an equation for measuring crack length by BFS (5) using finite element analysis (FEA).

$$A = EWB\left|\frac{\epsilon}{P}\right| \quad \text{equation 1.}$$

$$U = \frac{1}{A^{1/2}+1} \quad \text{equation 2.}$$

$$a/W = C_0 + C_1U + C_2U^2 + C_3U^3 + C_4U^4 + C_5U^5 \quad \text{equation 3.}$$

Where P the applied load; E is the Young modulus; A is the normalized compliance; U is the polynomial variable; and C_i coefficients that can be found in (1, 4, 5, 13).

In the equation 1, ϵ ratio is measured experimentally and so A is calculated. Once determined the value of A, the U value can be found using equation 2 and so the value of a/W is obtained by equation 3. These equations were tested in the present paper and a very good match was achieved. Table 3 presents the crack-length/width (a/W) ratio obtained by BFS (a_{BFS}/W) and the same parameter measured by optical microscopy (a_{MO}/W). Corrections in the crack length were not necessary, because significant crack tunnelling did not occur (17, 18), so the optical microscope measurement can be used as reference of crack length. As seen in table 4 a very satisfactory crack length is measured by BFS.

INSERT TABLE 4

Concerning the use of BFS for crack length measurement, figure 7 presents the da/dN plot including the near threshold region. This test was performed under constant load and its setup is presented in table 5:

INSERT TABLE 5

INSERT FIGURE 7

As it can be seen, very low values of crack length can be measured using BFS and good agreement was obtained with the reference curve extracted from the literature (19). Similar fatigue tests were performed in a corrosive medium containing 3% NaCl. Table 6 shows typical errors occurred during the tests for different crack lengths.

INSERT TABLE 6

As it can be seen by table 4 and 6, for air and in corrosive environment, the % error was very small. Furthermore, a comparison involving BS 7910 and LNDC results in air are shown in figure 8.
INSERT FIGURE 8

Excellent agreement was achieved using BFS validating the technique to monitor crack propagation even in corrosive medium. Moreover, the results in corrosive environment showed less dispersion than the test results in the air. For acid medium, it should be important to test the use of BFS in presence of hydrogen. Indeed, hydrogen could eventually permeate until the strain gauges' areas and introduce damages in the region where the strain gauges is placed, inducing error in the measurements. The effect of hydrogen permeation was tested using a C(T) sample with a strain gauge positioned on the back face and protected by the

coating [21]. Then, the sample was introduced into a cell containing 3% NaCl. The strain gauge signal was monitored during 108 ks. After this time, the sample was polarized at -1,300 mV (SCE) (mV (SCE): voltage measured versus saturated calomel electrode, as reference) maintaining the acquisition of strain data (ε) for more 864ks approximately. As it can be seen in Figure 9, it was not observed significant changes in measurement during the polarization, which means that the crack length measurement using BFS protected by the coating is adequate for corrosion-fatigue testing, even in presence of hydrogen.

INSERT FIGURE 9

Finally, the pressure effect on the measurements should be tested and the samples were submitted to high-pressure and the results are presented in table 7.

INSERT TABLE 7

From these results, it can be concluded that the use of BFS is adequate for corrosion-fatigue tests even in high-pressure medium as well in presence of hydrogen. It is now necessary to find the parameters for a similar equation proposed by (5), equation 3 above. This work was done using FEA and an excellent agreement was achieved, as it is shown in table 8 and figure 10 and now a similar simulation must be done for EFS.

INSERT TABLE 8

INSERT FIGURE 10

EFS simulation parameters obtained by FEA

As above seen, the parameters obtained by FEA appear to be very satisfactory for crack length measurement, and an EFS curve calibration must be now adjusted. First, it is necessary to find the best location to put the strain gauge to be used in the FEA. Twelve positions were tested and two factors have been analysed: the sensitivity (quality of the signal) and the easiness of the position to be reached (to be coated for example). Regarding sensitivity, candidates were selected whose ϵ_{EFS}/ϵ average values were the highest possible. These results are shown in figure 11 for crack lengths from 0.2 until 0.75.

INSERT FIGURE 11

By the criterion of sensitivity, two of the twelve strain gauges stood out, namely as 4 and 5-positions. In both positions, it can be seen that ϵ_{EFS}/ϵ ratio was higher than the average, allowing a better load resolution. Note, however, that this ratio tends to zero from the *a/W* equals to 0.65, thus, the calibration curve is validated for the *a/W* range 0.20-0.65. Regarding the easiness criterion, the strain gauge in-position 5 is the most suitable for applying a more robust coating, as it can be necessary in aggressive corrosion-fatigue tests. Thus, the strain gauge chosen was the one from position 5, and all results now will be related with this strain gauge.

Results using EFS to measure the load.

The equation 3 above shows the crack length related with *A*. As it had been previously shown (tables 4 and 6), the equation 3 gives correctly the crack length, but it depends on ϵ/P ratio, in

other words, a load cell until now is required to determine the crack length. The use of EFS in the present paper has been proposed exactly to eliminate the load cell in the tests. Figure 12 shows the plots of $|\epsilon|$ versus. $|\epsilon_{EFS}|$. It is clear that the relationship between the angular coefficients, $m = \epsilon / \epsilon_{BFS}$, increases with the crack length. It is possible to use the values of m to compute the load by using mathematical equations to be adjusted.

INSERT FIGURE 12

Indeed, the $\epsilon / \epsilon_{EFS}$ ratios, used to determine the crack length, now it will be adjusted using equations 4, 5 and 6, similar to those previous equations 1, 2 and 3:

$$m = \epsilon / \epsilon_{EFS} \quad \text{equation 4.}$$

$$M = \frac{1}{m^{1/2} + 1} \quad \text{equation 5.}$$

$$a/W = C_0 + C_1 M + C_2 M^2 + C_3 M^3 + C_4 M^4 + C_5 M^5 \quad \text{equation 6.}$$

The coefficients of the equation 6 were determined by a calibration curve, using FEA, and the following values were achieved for an X65 steel:

$C_0 = -1.1845$; $C_1 = 21.7500$; $C_2 = -91.8220$; $C_3 = 179.1000$; $C_4 = -169.7900$; $C_5 = 60.5590$;

for $0.20 \leq a/W \leq 0.65$.

The results of FEA and the experimental test performed in triplicate are seen in figure 13.

INSERT FIGURE 13

The above methodology makes unnecessary the use of a load cell in fatigue tests since, once the crack length is obtained using equation 6, the applied load working directly on the specimen can be predicted using the equation 7, gotten from the literature (5).

$$P_{Pred} = \frac{\left(1 - \frac{a}{W}\right)^2 . B.W.E.|\epsilon|}{1{,}41 - 1{,}462\frac{a}{W} + 20{,}45\left(\frac{a}{W}\right)^2 - 26{,}83\left(\frac{a}{W}\right)^3 + 11{,}45\left(\frac{a}{W}\right)^4} \quad \text{equation 7.}$$

Figure 14 shows the relationship between the load measured by a calibrated load cell and the values gotten by equation 7. By this plot it is possible to see that the P_{PRED} values (predicted load) are very near to the value measured by a load cell (P from load cell). Furthermore, predicted load plot is a perfectly straight as shown by equation 7, where P is a linear function of ϵ for a predetermined crack length. In contrast, P from load cell versus ϵ is subject to noises. Values of $A \pm 2\%$ of the reference load P from load cell was taken to obtain values of upper and lower limits, i.e., they are respectively equal to the product of P from load cell times 1.02 and 0.98.

INSERT FIGURE 14

A more detailed relationship is presented in tables 9 and 10 for a larger range of crack length.

INSERT TABLE 9

INSERT TABLE 10

In order to exemplify that higher than 2% error could be caused using a load cell in a high pressure tests, figure 15 presents a scheme of the problem. In this example, it was considered 250 N constant friction, autoclave under 200 bar, having an inch diameter shaft, controlled by a load cell using range load of 3 kN and a load ratio, *R*, equals to 0.25 in a frequency of 1 Hz.

INSERT FIGURE 15

As it is shown in figure 16 the sample load response presents an offset regarding the load cell, as well as a discontinuity at the peaks of the sine wave, caused due to the sign change of the frictional force showed in figure 15. Furthermore, in the practice, some of these parameters are not constants, and depending on, for example, the material, load range, total pressure and frictional force, so the difference will increase considerably.

INSERT FIGURE 16

In this example, some error obtained were more than 4%, even after eliminate the offset. That is why it is not a good practice using a correct factor as some fatigue machine companies have employed commonly in corrosion fatigue high pressure tests.

Intending confirm experimentally the issue addressed here, it were conducted four fatigue tests in a pressure vessel. Thus, the BFS technique was used within the linear elastic regime in order of verifying any discrepancies between the load values measured by the load cell and the corresponding deformation of the strain gauge depending on the internal pressure of the vessel, namely 0, 5, 10 and 50 bar. It is easy to see through Figure 17 that the internal pressure in the vessel causes a discrepancy between these values, proving that the load cell has considerable errors when the test is performed under high pressure.

INSERT FIGURE 17

Despite this problem, it is noticed by the results obtained at the present paper that the standards (1 and 21) were respected in the crack length range studied and the load applied directly under the specimen can be measured correctly even when subjected to high pressures.

The results above should now be improved working experimentally with different geometric dimensions of the C(T) specimen (*B* and *W* values), as well as other materials presenting different *E* values, therefore it could be possible to adjust a normalized equation as done in (4,5). Another complementary work is to extend this approach for other type of fatigue test specimens, like SEN(T), a single edge notch tension sample, and SEN(B), a single edge notch bending specimen.

Conclusions

In this paper it was shown that strain gauges can be used to monitor the crack propagation and, at the same time, the load imposed during a corrosion-fatigue test. It is an innovation in fatigue tests using a compliance technique. This feature is essential for tests to be performed in high-pressured system using autoclaves. A normalized equation that can be used for C(T) samples is in progress and later other useful samples like SEN(T) and SEN(B) will also be tested using the same methodology here proposed.

References

(1) ASTM, E647: **Standard Test Method for Measurement of Fatigue Crack Growth Rates** 1, 1999.
(2) ISO 12108, Metallic materials - Fatigue testing - Fatigue crack growth method, 2002.
(3) A. **International Handbook Committee, Fatigue and Fracture**, in: ASM Handbook. Vol. 19, 1996: pp. 500–506.
(4) W.F. Deans, C.E. Richards, A simple and sensitive method for monitoring crack and load in compact fracture mechanics specimens using strain gauges, J. Test. Eval. 7 (1979) 147–154.
(5) J.C. Newman, Y. Yamada, M. a. James**,** Back-face strain compliance relation for compact specimens for wide range in crack lengths, **Eng. Fract. Mech**. 78 (2011) 2707–2711.
(6) W.J.D. SHAW, W. ZHAO, Back face strain calibration for crack length measurements, J. Test. Eval. 22 (n.d.) 512–516.
(7) W.T. Riddell, R.S. Piascik, A Back Face Strain Compliance Expression for the Compact Tension Specimen, **NASA TM**. (1998).
(8) R. R. A. Garcia, A. Beserra, D.P. Dias, K. S. Assis, O. R. Mattos, Back-face strain compliance relation for SEN (B) specimens for wide range in crack lengths, **NACE**, 2015.
(9) R. Yuan, The relationships between weight functions, geometric functions, and compliance functions in linear elastic fracture mechanics, 2007.
(10) M. Tarafder, S. Tarafder, V.R. Ranganath, Location independent CCL relations for standard fracture mechanics specimens**, J. Fatigue**. 19 (1997) 635–640.
(11) A. Saxena, J. S.J. Hudak, Review and extension of compliance information for common crack growth specimens, Int**. J. Fract**. 14 (1978) 453–468.
(12) D.C. Maxwell, Strain based compliance method for determining crack length for a C(T) specimen, **AFWAL**-TR-87-4046. (1987).
(13) ASTM, E1820: **Measurement of Fracture Toughness** 1, 2001.
(14) ANSYS Inc., U.S.A. **Ansys Mechanical APDL Element Reference**, 2011.
(15) S.E. Benzley, Representation of singularities with isoparametric finite elements, Int. J. Numer. Methods Eng. 8 (1974) 537–545.
(16) G.P. Anderson, V.L. Ruggles, G.S. Stibor, Use of finite element computer programs in fracture mechanics, Int. **J. Fract**. Mech. 7 (1971) 63–76.
(17) BS-7448, **Fracture mechanics toughness tests Part 4; Method for determination of fracture resistance curves and initiation values for stable crack extension in metallic materials**, 1997.

(18) ASTM, E 399: **Standard Test Method for Linear-Elastic Plane-Strain Fracture Toughness K Ic** of, 2011.
(19) BS-7910, **Guide to methods for assessing the acceptability of flaws in metallic structures**, 2005.
(20) M. a. V. Devanathan, Z. Stachurski, The Adsorption and Diffusion of Electrolytic Hydrogen in Palladium, **Proc. R. Soc. A Math. Phys. Eng.** Sci. 270 (1962) 90–102.
(21) ASTM, E4: **Standard Practices for Force Verification of Testing Machines**, 2014.

*** * ***

Tables

Table 1 - Chemical composition (%) of API X65 steel used in tests and simulation.

C	Si	Mn	V	Ti	N (max)	Fe
0.09	0.30	1.65	0.050	0.018	0.009	bal

Table 2 - Technical information of the two coatings used in the tests.

Item	Elastomer	Ceramic coating
Shear strength in steel (bar)	30	290
Tensile strength (bar)	190	790
Compressive strength (bar)	-	1480
Tear strength (pli, pounds per linear inch)	130	-
Specific electrical resistance (Ω.cm)	-	$5.1x10^{14}$
Hardness	95 (Shore A, DIN 53505)	28 (Brinell, DIN 50351)
Electrochemical corrosion (DIN 50900)	none	none

Table 3 - Positioning of the strain gauges used in the analysis by finite elements.

Strain gauge	Position (mm)	Position-to-width ratio (mm/mm)
1	1.25	0.021
2	6.25	0.104
3	11.25	0.188
4	16.25	0.271
5	21.25	0.354
6	26.25	0.438
7	31.25	0.521
8	36.25	0.604
9	41.25	0.688
10	46.25	0.771
11	51.25	0.854
12	56.25	0.938

Table 4 - Experimental errors occurred in crack length measurement of fatigue tests under atmospheric air (20 ºC ± 2 ºC), using BFS technique.

a_{BFS}/W	0.202	0.216	0.234	0.252	0.267	0.285
a_{MO}/W	0.203	0.217	0.232	0.250	0.268	0.284
% error	-0.7%	-0.6%	0.9%	0.8%	-0.5%	0.5%
a_{BFS}/W	0.301	0.317	0.336	0.352	0.369	0.384
a_{MO}/W	0.300	0.318	0.338	0.354	0.371	0.386
% error	0.4%	-0.2%	-0.6%	-0.5%	-0.5%	-0.6%
a_{BFS}/W	0.420	0.454	0.485	0.517	0.550	0.583
a_{MO}/W	0.419	0.454	0.486	0.516	0.552	0.585
% error	0.3%	0.1%	-0.2%	0.2%	-0.4%	-0.3%
a_{BFS}/W	0.617	0.651	0.684	0.702	0.719	0.725
a_{MO}/W	0.615	0.648	0.680	0.700	0.720	0.724
% error	0.4%	0.4%	0.6%	0.3%	-0.1%	0.1%

Table 5 - Fatigue test parameters to obtain the curve *da/dN* vs. Δ*K* shown in Figure 6.

Test Parameter	**Pre-crack**	**Fatigue test**
Environmental	atmospheric air	atmospheric air
Load range, $\Delta P\ (N)$	2000	2000
Load ratio, R	0.50	0.50
Initial stress intensity factor, ΔK_0 (MPa.m$^{1/2}$)	3.49	3.93
Final stress intensity factor, ΔK_f (MPa.m$^{1/2}$)	3.93	29.63
Frequency, f (Hz)	50.00	11.00
Initial crack length, a_0 (mm)	12.00	14.51
Final crack length, a_f (mm)	14.51	45.68 (47.00) *
Initial crack-length-to-width ratio, $a/W_{inicial}$	0.2	0.242
Final crack-length-to-width ratio, a/W_{final}	0.242	0.761 (0.783)

** Plasticity criterion has been violated at a = 45.68 mm, but the acquisition of da/dN data still remained up* a_f *equals to 47.00mm* (1).

Table 6 - Experimental errors occurred in crack length measurement of four corrosion-fatigue tests in 3% NaCl solution (20 ± 2 ºC), using BFS, under 0.2 Hz.

Experimental Test 1	a_{BFS}/W	0.201	0.306	0.334	0.422	0.543	0.603
	a_{MO}/W	0.202	0.308	0.333	0.423	0.545	0.605
	% error	-0.5%	-0.6%	0.3%	-0.2%	-0.4%	-0.3%
Experimental Test 2	a_{BFS}/W	0.202	0.251	0.351	0.45	0.552	0.653
	a_{MO}/W	0.201	0.252	0.352	0.449	0.553	0.65
	% error	0.5%	-0.4%	-0.3%	0.2%	-0.2%	0.5%
Experimental Test 3	a_{BFS}/W	0.200	0.302	0.402	0.501	0.601	0.702
	a_{MO}/W	0.199	0.301	0.404	0.499	0.601	0.705
	% error	0.5%	0.3%	-0.5%	0.4%	0.0%	-0.4%
Experimental Test 4	a_{BFS}/W	0.202	0.304	0.401	0.500	0.6	0.698
	a_{MO}/W	0.203	0.306	0.402	0.498	0.597	0.699
	% error	-0.5%	-0.7%	-0.2%	0.4%	0.5%	-0.1%

Table 7 - Test conditions and results of C(T) the high-pressure tests.

Teste Number	**1**	**2**	**3**	**4**	**5**	**6**	**7**	**8**
Pressure (bar)	50	100	150	190	220	260	280	320
Time (h)	1	1	1	1	1	1	1	60
Result	A*	A	A	A	A	A	A	A

* approved, i.e., no infiltration was detected and the BFS signal did not change.

Table 8 - Comparison between the equation 3 coefficients

obtained by Deans (4), Newman (5), and LNDC.

Researcher	C_0	C_1	C_2	C_3	C_4	C_5	***a/W Range***
Deans	1.0141	-2.0347	-0.9992	-13.4463	79.7210	-102.8550	0.3 – 0.7
Newman	1.0033	- 2.3500	1.3694	- 15.2940	63.1820	- 74.4200	0.2 – 0.95
LNDC/ UFRJ	1.0008	-1.9734	-3.3128	7.9799	12.6840	34.2300	0.2 – 0.95

Table 9 - Experimental errors found in the load measured by EFS compared with a calibrated load cell during the two first experimental tests.

P_{LC} (kN)	P_{pred} (kN)	% error	P_{pred} (kN)	% error	P_{pred} (kN)	% error	P_{pred} (kN)	% error
	a =13 mmm		*a =14 mmm*		*a =14.5 mmm*		*a =15 mmm*	
15.50	15.30	1.30	15.24	1.36	15.74	-1.51	15.38	0.47
14.27	14.03	1.68	14.06	1.48	14.23	-1.19	14.23	0.50
13.01	12.76	1.97	12.84	1.65	13.26	-1.02	13.04	0.45
11.86	11.63	1.93	11.69	1.66	12.10	-0.96	11.83	0.56
10.69	10.50	1.75	10.50	1.67	10.90	-1.07	10.63	0.56
9.49	9.39	1.01	9.38	0.93	9.69	-1.84	9.46	0.42
	a =16 mmm		*a =17 mmm*		*a =18 mmm*		*a =19 mmm*	
12.41	12.26	1.21	12.32	0.87	12.23	1.35	12.34	1.00
11.49	11.30	1.66	11.34	1.18	11.40	1.73	11.54	1.39
10.50	10.32	1.72	10.36	1.39	10.43	1.53	10.58	1.20
9.57	9.40	1.83	9.43	1.48	9.53	1.77	9.64	0.87
8.64	8.49	1.67	8.55	1.05	8.58	1.62	8.74	1.62
7.66	7.59	0.90	7.60	0.51	7.59	1.07	7.68	0.97
	a =20 mmm		*a =21 mmm*		*a =21.5 mmm*		*a =22 mmm*	
10.35	10.27	0.82	10.33	0.64	10.28	1.16	10.28	0.77
9.56	9.45	1.18	9.47	1.03	9.57	0.76	9.44	1.41
8.74	8.62	1.36	8.64	1.21	8.72	0.51	8.65	1.26
7.99	7.90	1.09	7.86	1.13	8.02	0.49	7.83	1.30
7.10	7.01	1.29	7.11	0.95	7.13	0.75	7.08	1.20
6.36	6.32	0.66	6.36	0.48	6.45	1.33	6.31	0.65
	a =23 mmm		*a =23.3 mmm*		*a =23.6 mmm*		*a =24 mmm*	
8.37	8.31	0.73	8.39	1.38	8.40	1.50	8.34	0.56
7.76	7.67	1.11	7.79	1.19	7.80	0.97	7.65	0.95
7.06	6.97	1.26	7.11	0.98	7.09	1.11	6.98	0.73
6.44	6.35	1.34	6.47	0.93	6.48	1.15	6.36	1.08
5.79	5.72	1.18	5.83	1.21	5.82	1.15	5.72	0.91
5.13	5.10	0.52	5.16	0.96	5.25	1.91	5.13	0.26
	a =26 mmm		*a =26.3 mmm*		*a =26.66 mmm*		*a =27 mmm*	
7.12	7.13	0.09	7.12	0.11	7.11	0.02	7.05	0.15
6.57	6.57	0.21	6.56	0.45	6.58	0.40	6.58	0.47
6.03	6.04	0.38	6.03	0.59	6.05	0.56	6.02	0.55

5.48	5.47	0.45	5.47	0.62	5.48	0.59	6.47	0.93
4.93	4.94	0.30	4.94	0.45	4.93	0.35	5.45	0.60
4.38	4.39	0.31	4.38	0.15	4.39	0.21	4.41	0.12
	a =28 mmm		*a =28.5 mmm*		*a =29 mmm*		*a =30 mmm*	
6.57	6.57	0.01	6.59	-0.46	6.62	0.82	6.66	1.46
6.06	6.09	0.43	6.08	-0.11	6.10	0.50	6.14	1.16
5.55	5.57	0.45	5.55	0.14	5.60	0.35	5.65	1.00
5.04	5.06	0.48	5.04	0.09	5.08	0.48	5.12	0.90
4.53	4.55	0.36	4.42	-0.13	4.60	0.74	4.61	1.01
4.02	4.03	0.31	4.06	-0.80	4.07	1.18	4.10	1.84

Table 10 - Experimental errors found in the load measured by EFS compared with a calibrated load cell during the third experimental test.

P_{LC} (kN)	P_{pred} (kN)	% error	P_{LC} (kN)	P_{pred} (kN)	% error	P_{LC} (kN)	P_{pred} (kN)	% error
	a = 15.09mm			*a = 21mm*			*a = 25.8mm*	
12.39	12.35	0.38	10.31	10.35	-0.40	7.83	7.74	1.06
11.43	11.44	-0.05	9.51	9.50	0.08	7.35	7.37	-0.20
10.47	10.47	0.02	8.71	8.70	0.06	6.88	6.90	-0.37
9.51	9.49	0.25	7.91	7.88	0.32	6.40	6.44	-0.57
8.55	8.55	0.10	7.11	7.13	-0.27	5.93	5.84	1.56
7.59	7.54	0.73	6.31	6.31	-0.06	5.45	5.54	-1.56
	a = 30.6mm			*a = 35.4mm*			*a = 39mm*	
6.48	6.46	0.38	4.63	4.62	0.38	4.02	3.98	1.01
5.98	5.99	-0.11	4.28	4.30	-0.48	3.70	3.71	-0.25
5.48	5.49	-0.16	3.93	3.92	0.21	3.39	3.38	0.27
4.98	4.97	0.08	3.58	3.56	0.56	3.08	3.09	-0.55
4.48	4.50	-0.63	3.22	3.24	-0.44	2.76	2.78	-0.53
3.97	3.92	1.40	2.87	2.84	1.20	2.45	2.42	1.08

Figures

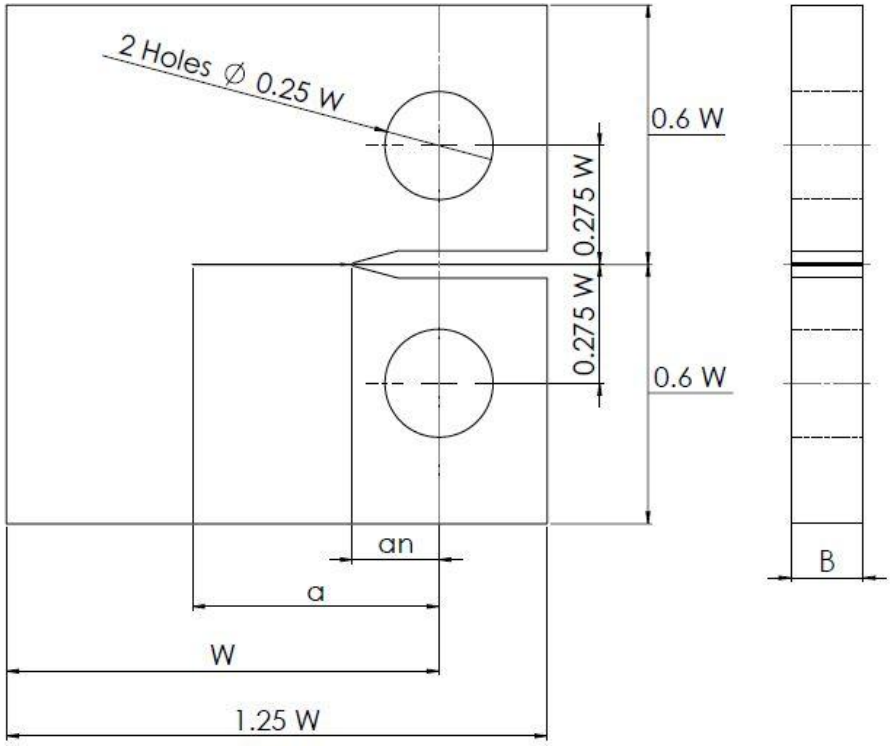

Figure 1 - Geometric dimensions of the specimen used in the experiments and Finite Element Analysis.

Where: *W*, sample width, = *60 mm B*, sample thickness, = *10mm*. Source: extracted from (1).

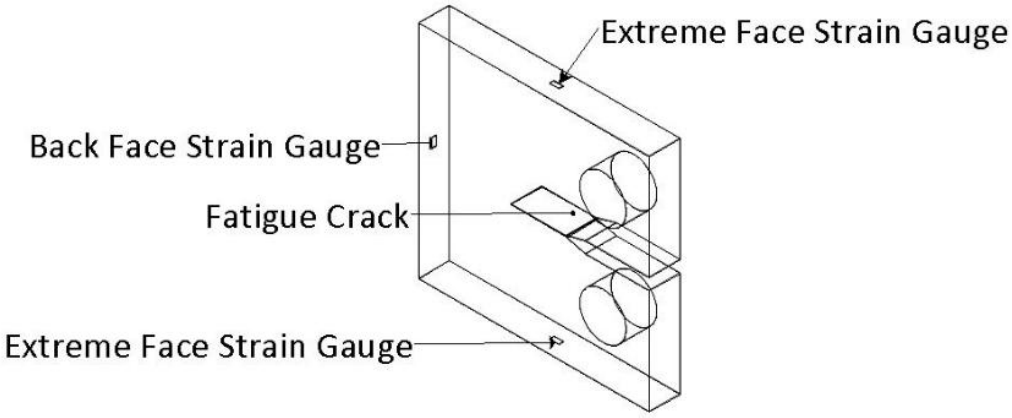

Figure 2 - Positioning of the strain gauges on C(T) specimen.

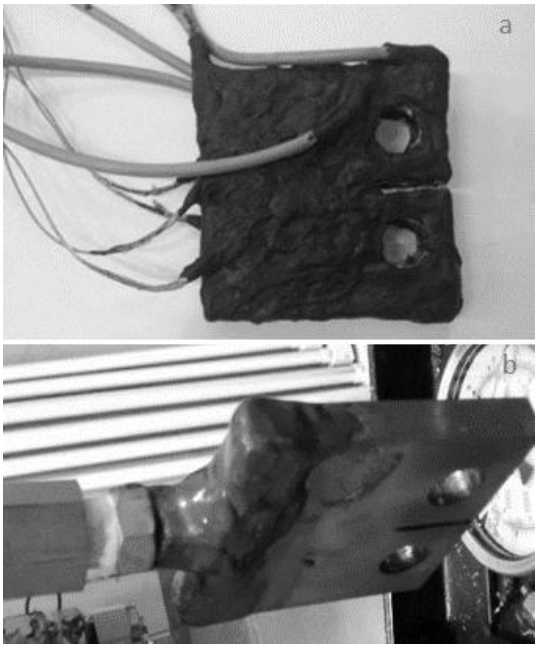

Figure 3 - Elastomer (a) and Ceramic coating (b) applied to the specimen.

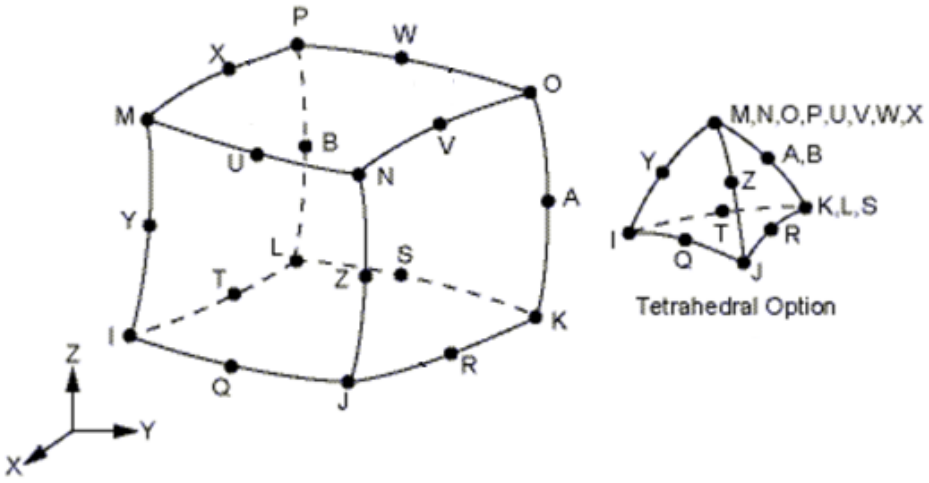

Figure 4 - Type and geometry element used in FEA.

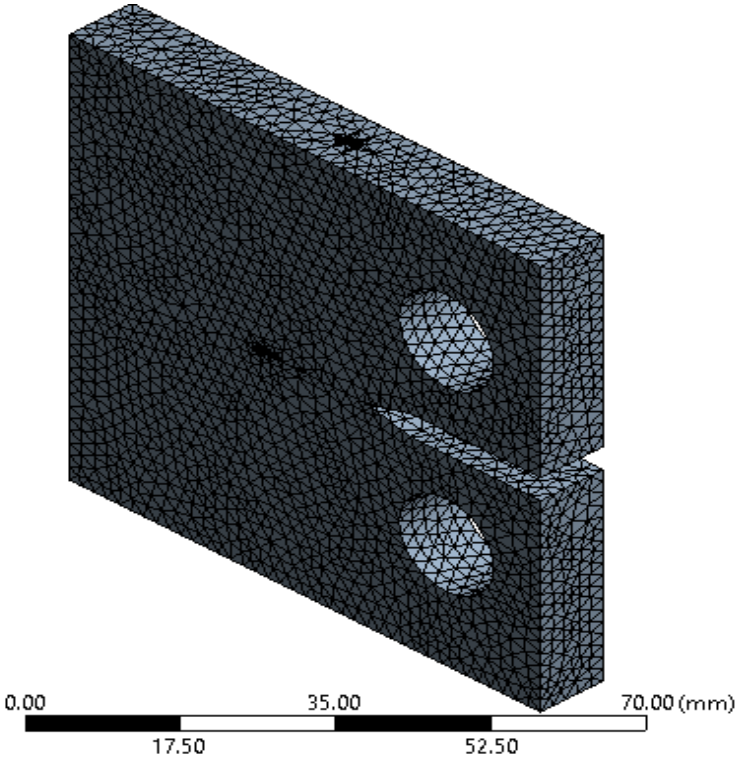

Figure 5 - Mesh type used in finite element simulation of the BFS.

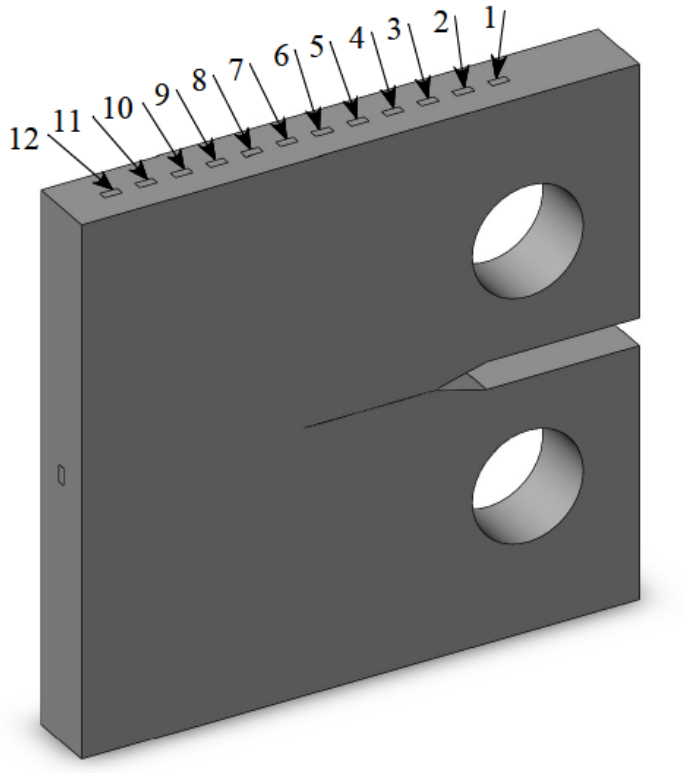

Figure 6 - Position of the strain gauges used in the analysis by finite elements.

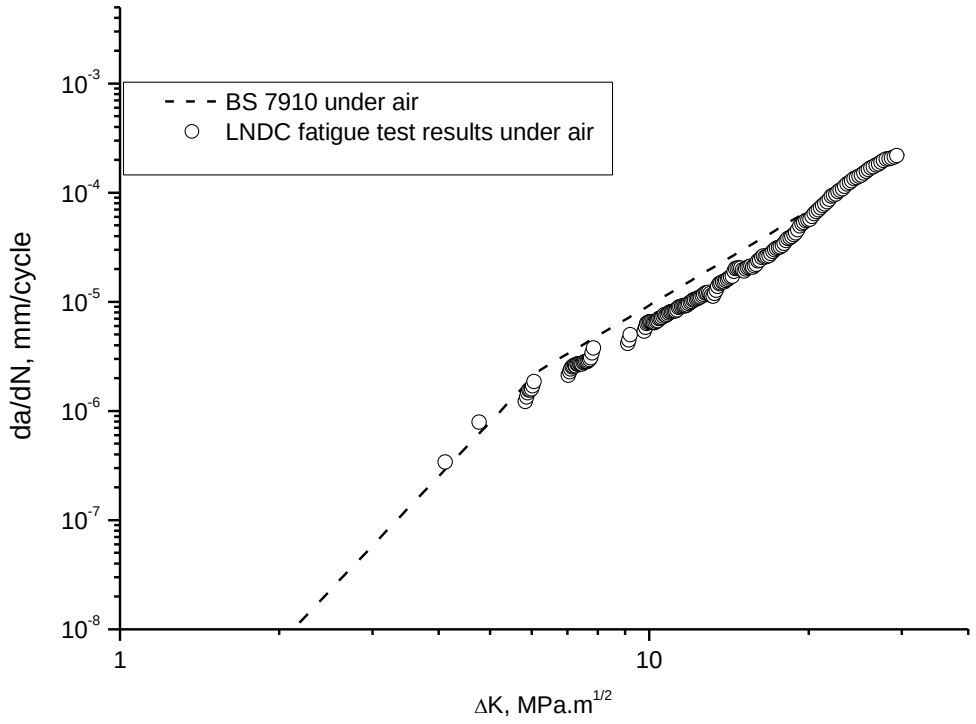

Figure 7 – *da/dN* versus ΔK curve, using the BFS technique and compared with the data from reference 13 in air condition.

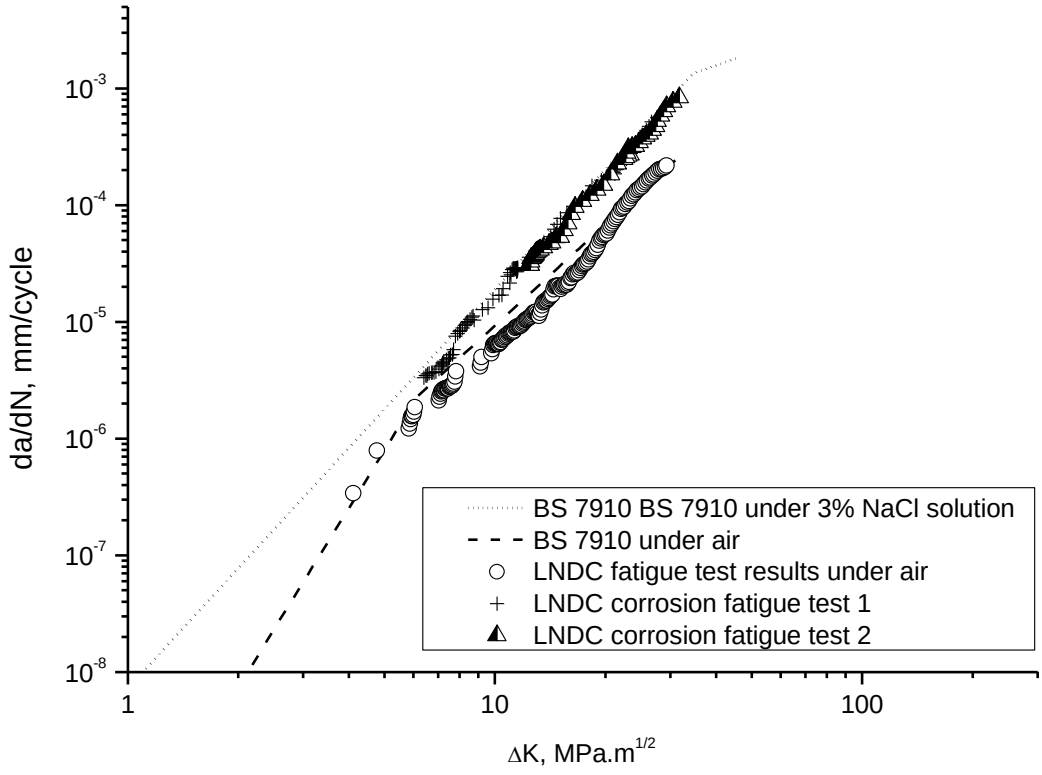

Figure 8 - *da/dN* versus ΔK curve, using the BFS technique and compared with the data from reference 13 in air condition and NaCl 3% solution (20 ± 2 ºC) in duplicate, under 0.2 Hz.

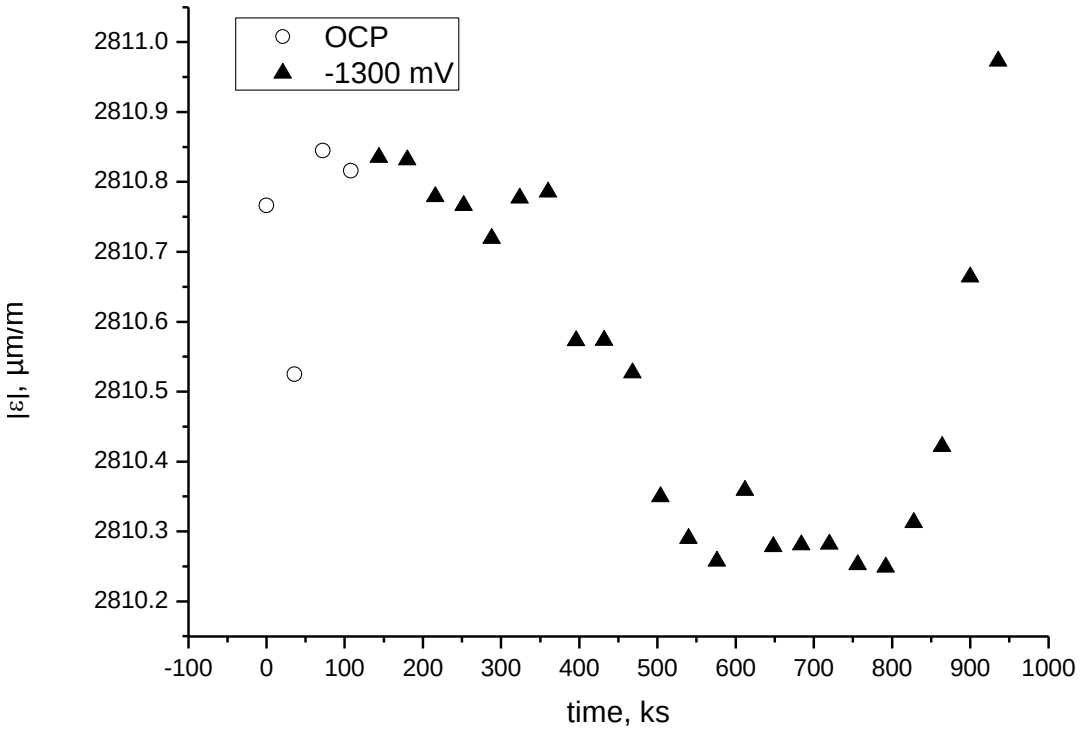

Figure 9 - Strain measurements on the back face of the C(T) specimen at open circuit potential (for 30hours) followed by a polarization at -1,300 mV (SCE) for approximately 10 days.

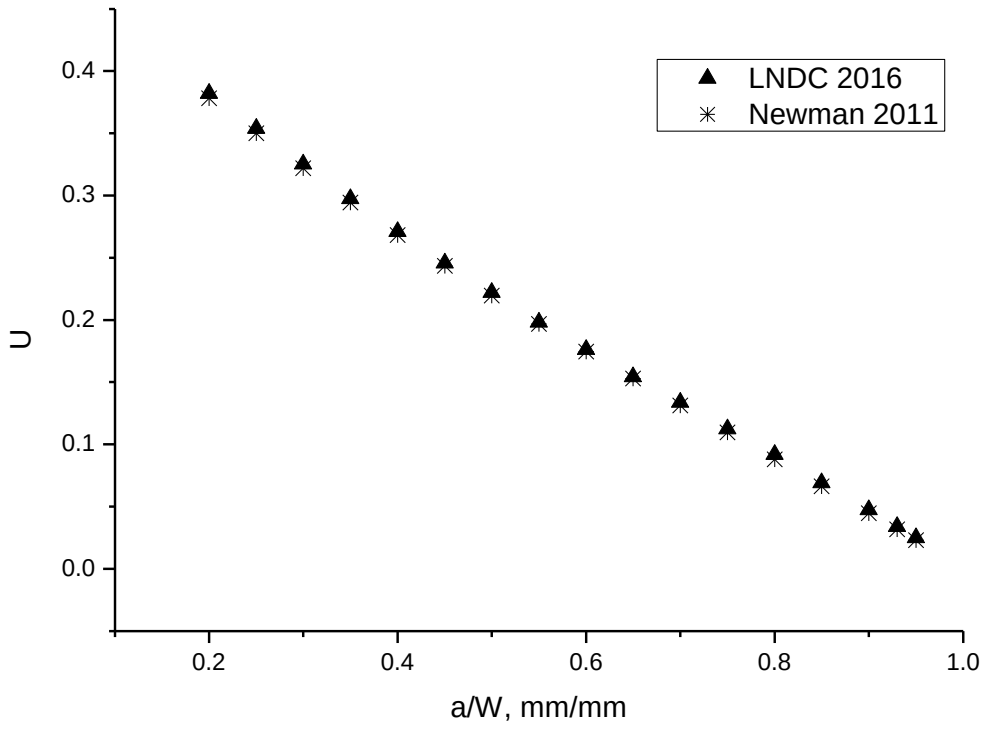

Figure 10 - Comparison between the results found in (4) and the methodology applied at LNDC.

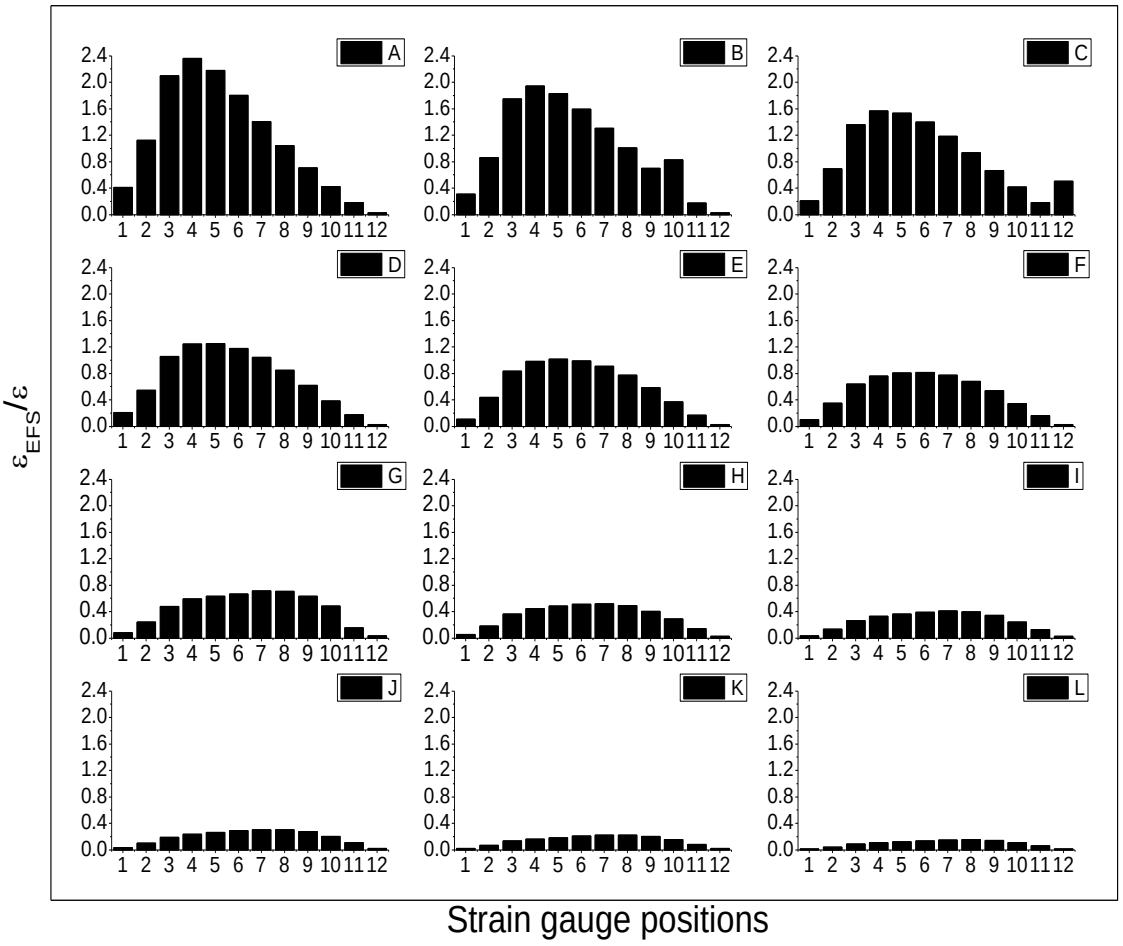

Figure 11 - ϵ_{EFS}/ϵ ratio values for different crack lengths, indicating what position the EFS has greater sensitivity, for *a/W* values from A until L, respectively equal to 0.25, 0.30, 0.35, 0.40, 0.45, 0.50, 0.55, 0.60, 0.65, 0.70, 0.75.

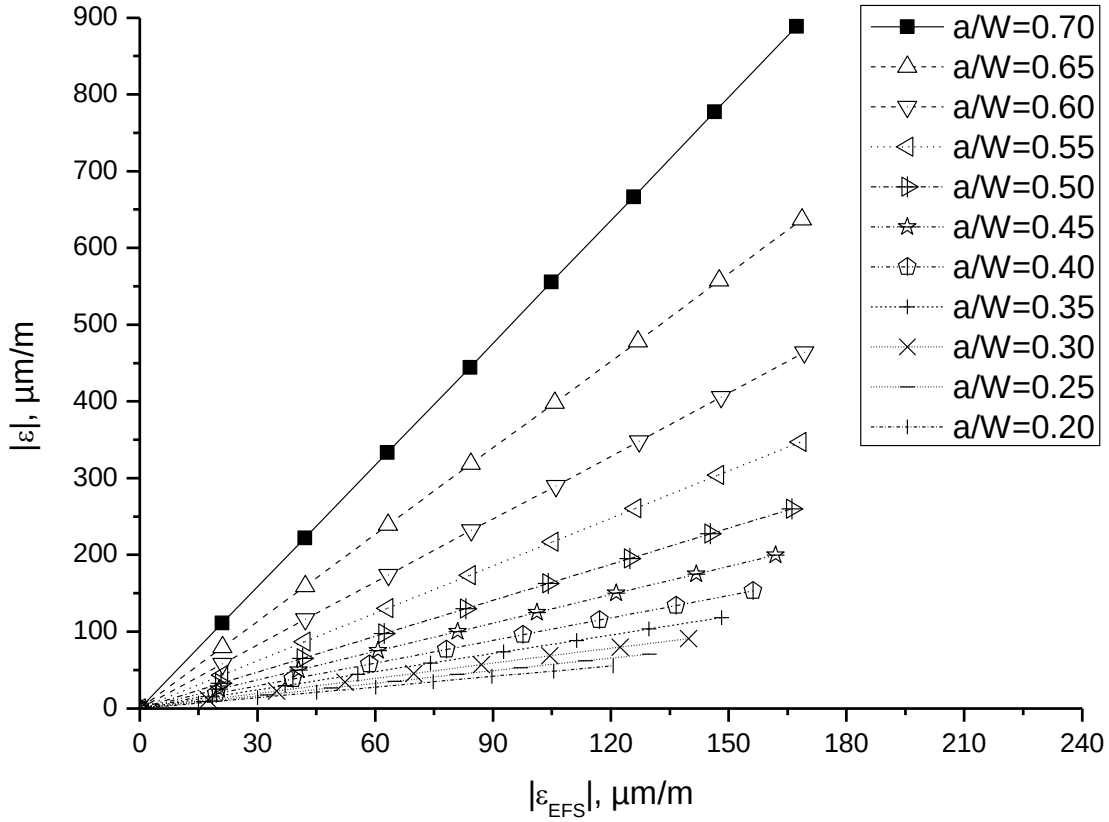

Figure 12 - Plot obtained by FEA, showing a linear relationship between EFS and BFS, whose slope varies as a function of crack length.

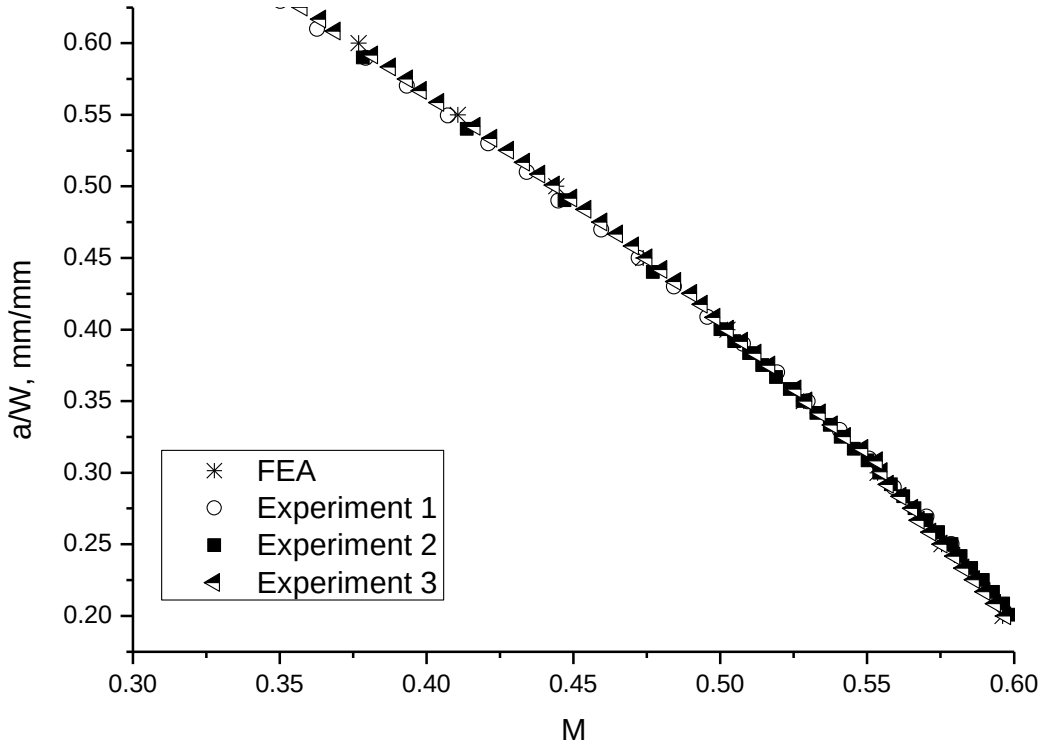

Figure 13 - Comparison of calibration curve obtained by FEA for obtaining *a/W* as function of *M* and two experimental tests.

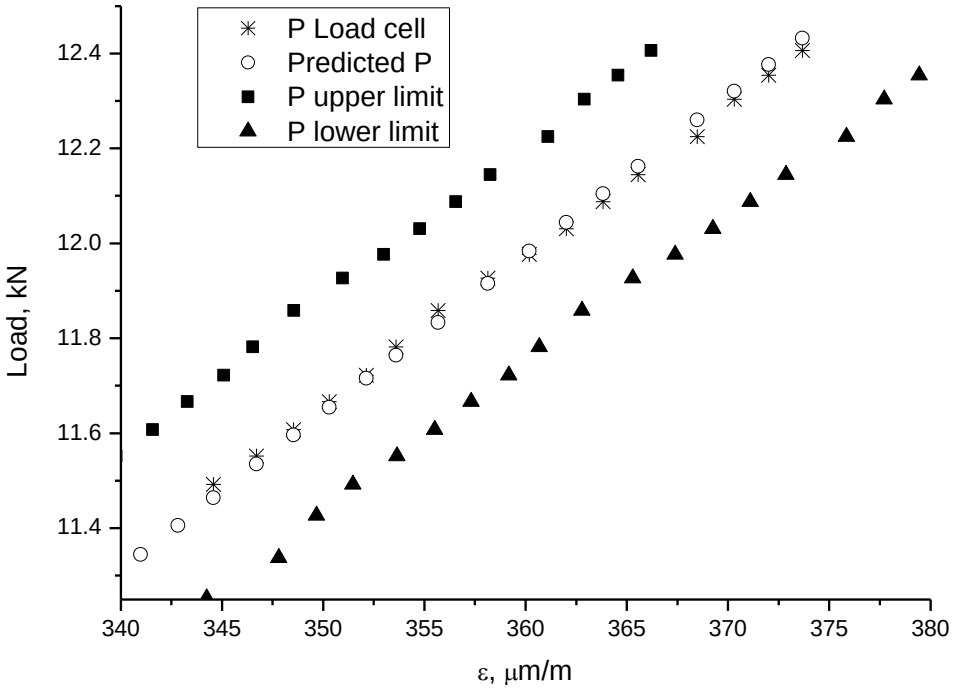

Figure 14 - Comparison between the measured load by the load cell and the predicted load by Eq. 7 for *a/W = 16.003 mm*

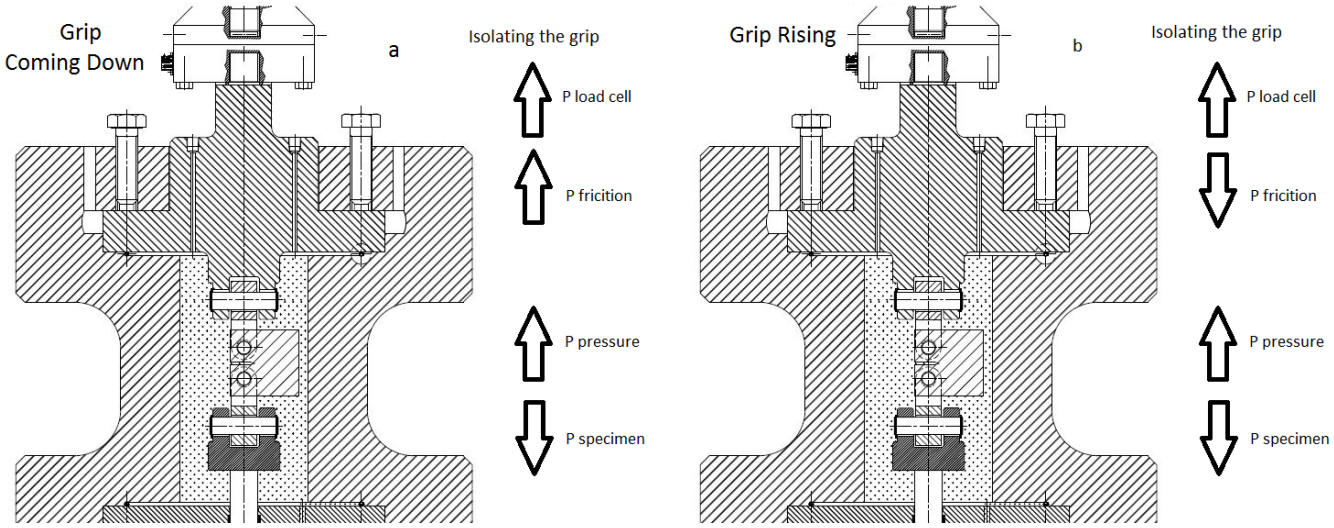

Figure 15 - Simplified scheme of the influence of the friction force and total pressure in a load cell controlled test.

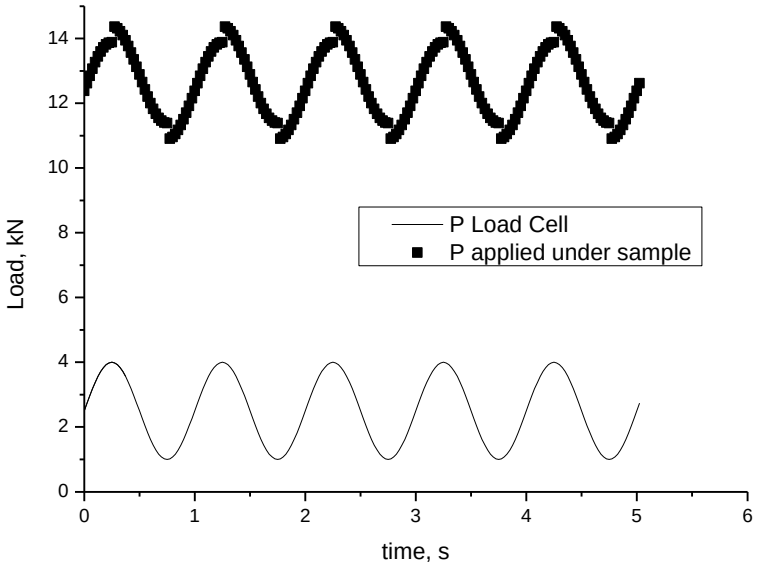

Figure 16. Comparison between the load directly applied on the specimen and the load applied by the load cell.

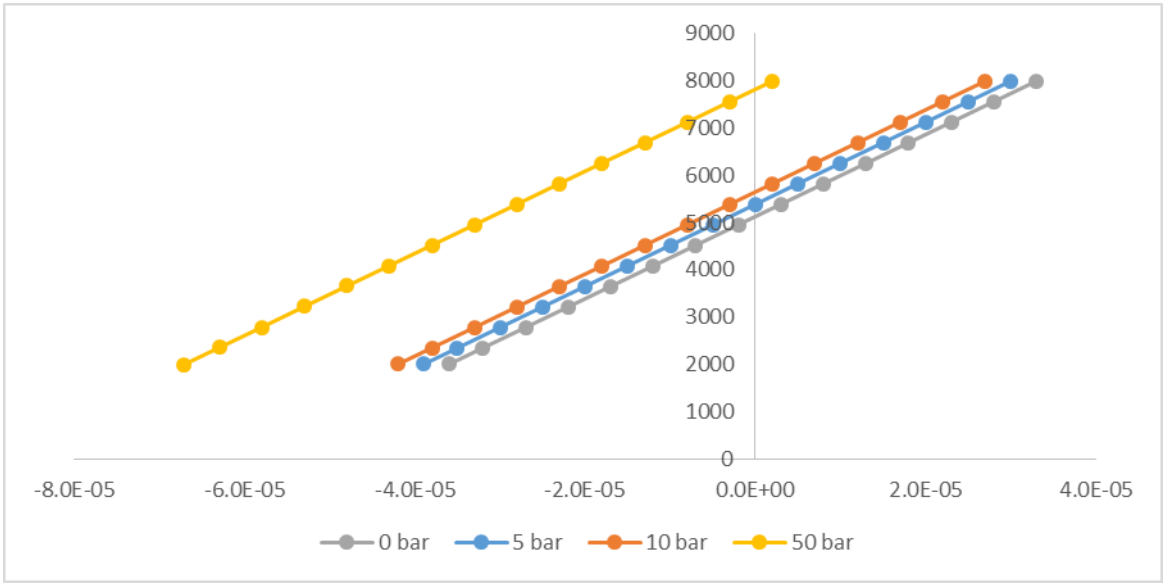

Figure 17. P VS curves ε presenting changes due to the internal pressure of the vessel.